ELECTROCHEMICAL STUDY OF CuSCN INORGANIC HOLE-TRANSPORT MATERIAL FOR SOLAR CELLS PREPARED BY ELECTRODEPOSITION FROM AQUEOUS SOLUTION

Zuzana VLČKOVÁ ŽIVCOVÁ, Věra MANSFELDOVÁ, Milan BOUŠA, Ladislav KAVAN

J. Heyrovský Institute of Physical Chemistry of the CAS, Prague, Czech Republic, EU

https://doi.org/10.37904/nanocon.2020.3727

Abstract

A comparative study is reported for electrodeposited copper(I) thiocyanate layers (ca. 500 nm) on two types of conductive/semiconductive substrates; i) carbon (boron-doped diamond_BDD, glass-like carbon_GC), and ii) carbon-free F-doped SnO_2 conducting glass (FTO). SEM and Raman evidence that electrodeposition from aqueous solution results in homogenous CuSCN layers with dominant thiocyanate ion bounded to copper through its S-end (Cu−SCN bonding), as in spin-coated CuSCN layers. Electrochemical impedance spectroscopy (EIS) confirms the *p*-type semiconductivity of layers with a flatband potential from 0.1 to 0.18 V vs. Ag/AgCl depending on the substrate type, and the acceptor concentration (N_A) of ~ 5 x $10^{20}$$cm^{-3}$ in all cases. The flatband potentials determined from Mott-Schottky plots (EIS) are in good agreement with the Kelvin probe measurements. The blocking quality of CuSCN layers was tested using $Ru(NH_3)_6^{3+/2+}$ redox probe. CuSCN deposited on BDD substrate exhibits better blocking properties compared to CuSCN deposited on FTO.

Keywords: Electrodeposition, CuSCN, hole transport material, electrochemistry, impedance spectroscopy

1. INTRODUCTION

Copper(I) thiocyanate (CuSCN) is a *p*-type semiconductor with wide band gap of ~3.9 eV, hole mobility 0.001−0.1 $cm^2 \cdot V^{-1} \cdot s^{-1}$ [1] and good optical transparency [2] applicable as a hole transport material (HTM) in dye-sensitized solid-state solar cells [3,4] and perovskite solar cells [5,6]. Cathodic electrodeposition from aqueous solution containing SCN^- and Cu^{2+} is one of the low-temperature deposition techniques for CuSCN layers [2,3,7-10] in addition to spray deposition [11], drop-casting [12] or spin coating [13]. The electrodeposition benefits from avoiding organic solvents (e.g. alkyl sulfides). EIS is a useful technique to study the double-layer structure and charge transfer at the electrochemical interface. Based on Mott-Schottky plot (MS) obtained by fitting impedance spectra using appropriate equivalent circuit, the flatband potential (E_{fb}), and acceptor (N_A) or donor (N_D) concentration can be determined [14]. However, the experimental flatband potentials depend on various factors, such as i) the presence of deliberately added dopants, ii) differences in the crystallographic orientation, iii) a difference in the pH of zero charge, etc. [15]. The flatband positions can be also determined from the work function using Kelvin probe measurements after the corresponding conversion to the electrochemical potential scale. This technique is based on measurement of changes in contact potential difference (CPD) between the studied surface and a reference probe [16,17]. Here we report the electrodeposition from aqueous solution of hole-transporting CuSCN layers under the same conditions on different types of substrates (boron-doped diamond as *p*-type semiconductor, FTO glass as *n*-type semiconductor, and glass-like carbon). The structure and electrochemical properties of the electrodeposited CuSCN layers were compared with those prepared by the spin-coating method [5].

2. EXPERIMENTAL

2.1. CuSCN layer preparation

CuSCN thin films were prepared by electrodeposition from aqueous electrolyte solution according Ni et al. [2] on: i) boron-doped diamond with B/C ratio of 1000 ppm (BDD 1000) and 4000 ppm (BDD 4000) as detailed

elsewhere [18], ii) glass-like carbon (GC, 3000C from Goodfellow, 400 μOhm/cm), and iii) F-doped SnO_2 conducting glass (FTO, TEC 15 from Libbey-Owens-Ford, 15 Ohm/sq). The electrodeposition of CuSCN was performed potentiostatically at -0.5V vs. Ag/AgCl for 30 minutes; Pt mesh was a counter electrode and Ag/AgCl with 3M KCl was a reference electrode. The electrolyte solution consists of cupric sulfate pentahydrate (99.9%, Sigma-Aldrich) and potassium thiocyanate (99.0%, Sigma-Aldrich) as precursors and TEA (99.0%, Sigma-Aldrich) as a chelating reagent for Cu^{2+} cations. Before electrodeposition, the $CuSO_4$/TEA + 0.1M KSCN solution was stirred for 1 h and then stored for 24 h.

2.2. Structural and chemical characterization

The surface morphology was investigated by field emission scanning electron microscopy (FESEM, S-4800 Hitachi). SEM images were acquired at an acceleration voltage of 3 kV at a working distance of 5-6 mm. Raman spectra were excited by 514 nm laser (power of 1 mW) and recorded by a Labram HR spectrometer (Horiba Jobin-Yvon) interfaced to an Olympus microscope (objective 100×). The spectrometer was calibrated by the F_{1g} mode of Si at 520.2 cm^{-1}. Kelvin probe measurements used KP020 instrument (KP Technology Ltd.). The gold probe was positioned close to the sample surface and the contact potential difference was measured. Work functions were calibrated using a freshly peeled-off highly oriented pyrolytic graphite; its work function was set to 4.6 eV [17]. All electrochemical measurements were performed in a three-electrode cell (working electrode: CuSCN film, counter electrode: Pt mesh, reference electrode: Ag/AgCl with 3M KCl). The electrolyte solution was 0.5M KCl (Sigma Aldrich) saturated with CuSCN (pH 6). Electrochemical experiments were carried out on AUTOLAB PGSTAT128N potentiostat (Metrohm) controlled by GPES4 software (cyclic voltammetry, CV) and FRA software (EIS). The electrochemical impedance spectra were measured at frequencies from 100 kHz to 0.1 Hz. Electrochemical test of blocking used of 0.5mM $[Ru(NH_3)_6]$ Cl_3 (Sigma Aldrich, 98%) in 0.5M KCl (Sigma Aldrich, ≥99%) sat. with CuSCN. Electrochemical measurements were carried out in a closed cell under argon atmosphere.

3. RESULTS AND DISCUSSION

3.1. Structural characterization of CuSCN layers

Figure 1A displays plan view of dense fine-crystalline morphology (trigonal crystallites) of homogeneously electrochemically grown CuSCN layer onto FTO substrate. The CuSCN layer thickness observed from cross sectional SEM image (**Figure 1B**) is about 550 nm and is comparable (same as morphology) with CuSCN layers prepared on BDD and GC substrate (not shown). The surface morphology of electrodeposited CuSCN layers is distinctly different from layers prepared by spin coating from diethyl sulfide solution and the crystal size is significantly larger [5].

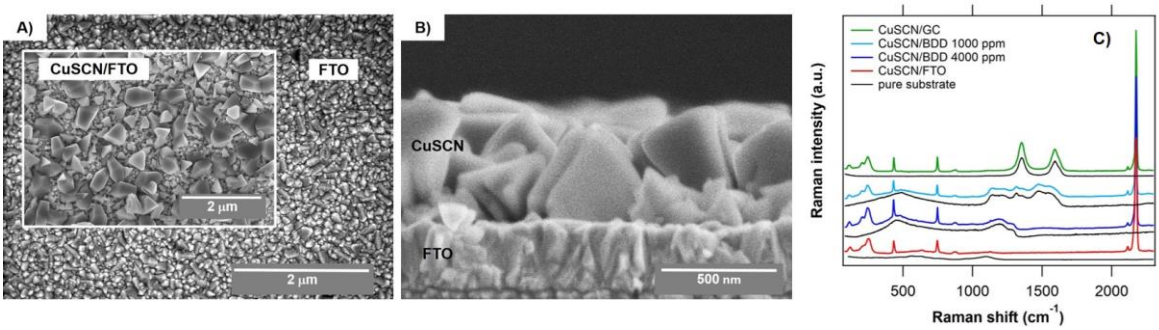

Figure 1 SEM (A_plain view, B_cross section) of CuSCN on FTO glass substrate (CuSCN/FTO). Inset of A) shows CuSCN on FTO substrate (background of the chart A). Chart C) shows the Raman spectra of CuSCN on GC (green line), BDD 1000 (light blue line), BDD 4000 (dark blue line), and FTO (red line) substrates. Black lines show the reference spectra of blank substrates. The spectra are offset for clarity.

Figure 1C shows Raman spectra of CuSCN layers deposited on different types of substrates (CuSCN/GC, CuSCN/BDD 1000, CuSCN/BDD 4000, and CuSCN/FTO). The Raman spectra of blank substrates are also shown for comparison. Independent of the substrate type the Raman spectra exhibit the same peak positions as the CuSCN films prepared by spin coating [5]. The peaks of C≡N stretching are located at higher frequency region, i.e. the weaker peak at 2115 cm^{-1} for isothiocyanate which is a less energetically favourable resonance form of SCN ion (Cu−NSC bonding) and the most intense peak at 2173 cm^{-1} for the second resonant form thiocyanate (Cu−SCN bonding). In the low frequency range region 100–1000 cm^{-1} where are located peaks indicating the presence of two possible SCN resonant forms are clearly visible the Raman peaks corresponding to the Cu-S stretching at 202 and 745 cm^{-1}, SCN bending at 431 cm^{-1}, and Cu-N stretching at 243 cm^{-1}.

3.2. Cyclic voltammetry (CV) and electrochemical impedance spectroscopy (EIS)

The CuSCN layers were electrochemically studied in 0.5M KCl sat. with CuSCN aqueous electrolyte solution in various potential ranges from -0.3V to 0.5V. The set of cyclic voltammograms (CVs) is illustrated in **Figure 2A** for CuSCN/BDD substrates, in **Figure 2B** for CuSCN/GC and CuSCN/FTO substrates. In all cases, with increasing potential window the capacitances, determined at 0 V and related to the projected geometric surface area, increase (**Figure 2C**) due to electrochemical reactions occurring on the electrode surface. As CuSCN is *p*-type semiconductor, cyclic voltammograms show no capacitive charging in cathodic direction, while with increasing positive potential the anodic current increases depending on the substrate type. For the anodic vertex potentials from 0.3 V to 0.5 V (**Figure 2D**), the increase of capacitance is more evident for CuSCN/FTO (0.6 mF/cm^2) and CuSCN/GC (0.8 mF/cm^2) than for CuSCN/BDD (0.3 mF/cm^2). This difference is caused by the variability of substrates used for CuSCN electrodeposition, i.e., the width of potential window (PW) of capacitive charging depends on the substrate type. The reason for the lowest capacitance values of CuSCN/BDD is that BDD has a wide electrochemical potential window in aqueous media (more than 3V for high quality and highly doped BDD) and low double-layer capacitance (< 12 $\mu F/cm^2$), as previously reported [14,18-21]. Depending on BDD film quality (sp^2 carbon content) and doping level (B/C ratio in the gas phase) we distinguish between high- and low-quality diamonds, as well as semiconducting (< 3 x 10^{20} B atoms cm^{-3} [22]) or metallic. For CuSCN electrodeposition, we used two types of BDD; 1) with lower quality and doping level denoted BDD 1000, and 2) high quality with high doping (BDD 4000). The structure and electrochemical properties of these BDDs were described in [18]. From the inset of **Figure 2C** it is obvious, that CuSCN/BDD 4000 layer exhibits slightly lower capacitance than the CuSCN/BDD 1000. The reason is the higher quality of the pristine BDD 4000 (compared to BDD 1000) containing no sp^2 carbon impurities (Raman spectrum in **Figure 1C**), where oxygen-containing groups are formed causing a decrease in the potential BDD window and an increase in background capacitive currents [18]. The GC (20 $\mu F/cm^2$ [5]) and FTO (30 $\mu F/cm^2$ [5]) substrates increase the capacitance of CuSCN layer in the whole range of potential windows compared to the BDD substrates due to various structure of surface containing oxygen groups where redox reactions occur.

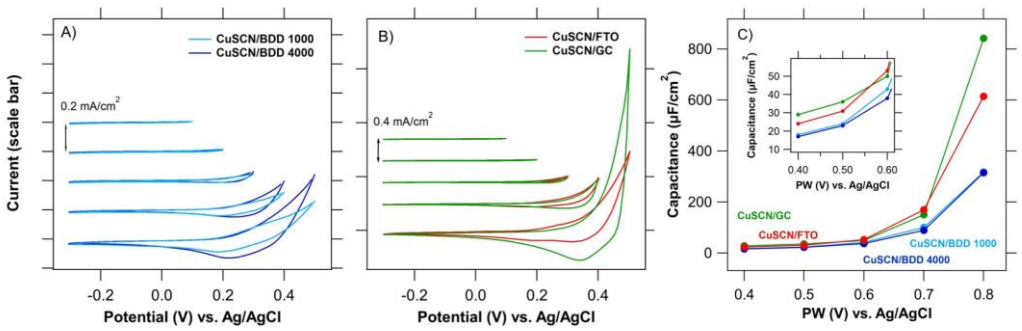

Figure 2 Cyclic voltammograms of CuSCN on A) boron-doped diamond (CuSCN/BDD 1000_light blue line, CuSCN/BDD 4000_dark blue line), B) glass-like carbon (CuSCN/GC_green line) and FTO glass substrate (CuSCN/FTO_red line). The scan rate of 100 mV/s. Plots in A) and B) are offset for clarity, but the current scale is identical for all voltammograms (see the scale bar). C) shows the capacitance of CuSCN in potential ranges from -0.3V–0.1V (PW=0.4) to -0.3V–0.5V vs. Ag/AgCl (PW=0.8) calculated from CVs in A) and B).

The blocking properties of electrodeposited CuSCN layer were tested using FTO and BDD 4000 substrates (**Figure 3**). In our previous work [5] the blocking function of spin-coated CuSCN was found to depend on details of spin-coating deposition. Here we used the same $Ru(NH_3)_6^{3+/2+}$ redox system due to suitable redox potential and stability of aqueous solution. **Figure 3** shows that CuSCN/BDD 4000 layer (blue line) has a better blocking function which is quantified as the relative pinhole area [23] (A_u/A_0) of 42% compared to CuSCN/FTO (red line) with A_u/A_0 = 64%, referenced to blank FTO (black line). The pinhole defect type A of the CuSCN layer was detected for both substrates [23]. The larger A_u/A_0 values obviously reflect the coarse morphology of our film (**Figure 1**) compared to spin-coated ones; nevertheless, this parameter is also known to depend dramatically on details of the spin-coating protocol [5].

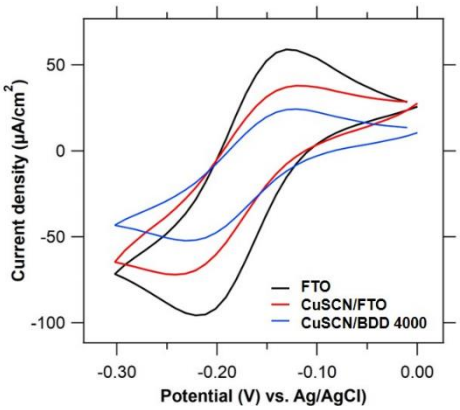

Figure 3 Cyclic voltammograms of CuSCN on FTO (red line) and BDD 4000 (blue line) substrates. Blank FTO substrate (black line) is shown for comparison. Electrolyte solution 0.5mM $Ru(NH_3)_6Cl_3$ in 0.5M KCl sat. with CuSCN (pH 6) and the scan rate 100 mV/s.

Figure 4 shows the Mott-Schottky plots determined from electrochemical impedance spectroscopy (EIS) and fitted using the RC equivalent circuits, where the space charge capacitance is represented by constant phase element (CPE) [14]. The negative slope of MS plots of CuSCN in all cases confirmed the *p*-type conductivity. Similarly, blank BDD (1000 and 4000) shows the *p*-type semiconducting behaviour (inset of **Figure 4A** and **Figure 4B**). For the calculation of the acceptor concentration N_A and flatband potential E_{fb} (**Table 1**), we used the Mott-Schottky equation [14]. The found flatband potentials depend on the substrate type, ie. the E_{fb} is lower in the case of carbon (BDD, GC) substrates compared to carbon-free FTO substrate. This trend is the same as in our previous work on spin-coated CuSCN layers [5]. For the CuSCN/BDD are the E_{fb} values as follows: 0.1 V (BDD 1000) and 0.13 V (BDD 4000) vs. Ag/AgCl compared to E_{fb} of blank BDDs (1.04 V for BDD 1000 and 1.3 V for BDD 4000) (**Figure 4A** and **Figure 4B**). The deposition on conductive GC substrate leads to the higher E_{fb} = 0.15 V (**Figure 4C**). Despite the fact, that the FTO is a *n*-type semiconductor (E_{fb} = -0.5 V vs. Ag/AgCl, **Figure 4D**), the *p*-semiconducting character of the CuSCN layer dominates and the flatband potential is 0.18 V vs. Ag/AgCl. This value is slightly higher, but still in good agreement with the value of 0.12 V measured on spin-coated CuSCN layers on FTO [5]. The acceptor concentrations of CuSCN layers on GC, BDD, and FTO are in the range of 4.7 to 5.4 x 10^{20} cm^{-3} (**Table 1**) comparable to spin-coated CuSCN layers [5]. KP measurements give the work function for CuSCN layers on FTO, GC, and BDD substrates as; 4.931 eV, 4.833 eV, and 4.575 eV, respectively. These work functions can be converted to the corresponding flatband potential. **Table 1** confirms that both techniques give well comparable data.

Table 1 The acceptor concentrations (N_A) and flatband potentials (E_{fb}) for CuSCN on various substrates (CuSCN/BDD 1000, CuSCN/BDD 4000, CuSCN/GC, and CuSCN/FTO) determined by electrochemical impedance spectra from Mott-Schottky (MS) plots and Kelvin probe (KP) method

	CuSCN/BDD 1000	**CuSCN/BDD 4000**	**CuSCN/GC**	**CuSCN/FTO**
N_A (cm^{-3}) (MS)	4.8 x 10^{20}	4.8 x 10^{20}	4.7 x 10^{20}	5.4 x 10^{20}
E_{fb} (V) vs Ag/AgCl (MS)	0.1 ± 0.01	0.13 ± 0.04	0.15 ± 0.02	0.18 ± 0.02
E_{fb} (V) vs.Ag/AgCl (KP)	-	0.14 ± 0.03	0.13 ± 0.03	0.24 ± 0.05

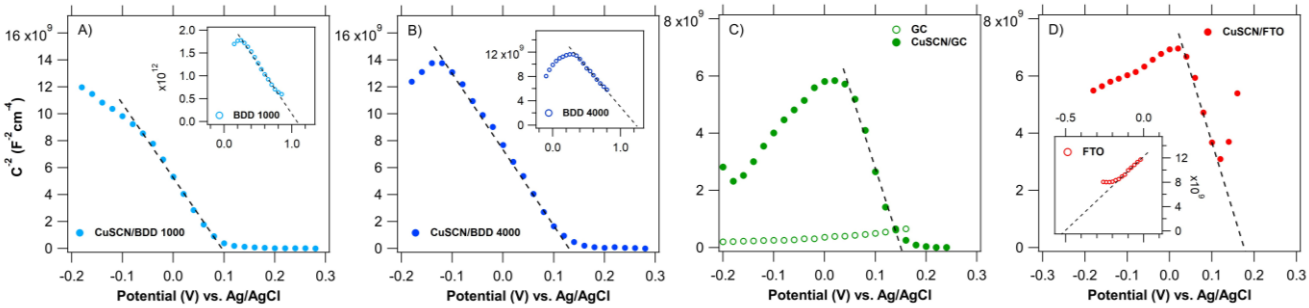

Figure 4 Mott−Schottky (MS) plots from EIS of CuSCN on A) boron-doped diamond CuSCN/BDD 1000_light blue full symbols, B) CuSCN/BDD 4000_dark blue full symbols, C) glass-like carbon (CuSCN/GC_green full symbol) and D) FTO substrate (CuSCN/FTO_red full symbols). The open symbols show the MS of substrates. Electrolyte solution was 0.5M KCl sat. with CuSCN (pH 6).

4. CONCLUSION

Electrochemical deposition on different substrates (boron-doped diamond, glass-like carbon, and FTO conductive glass) from aqueous solution yielded homogenous CuSCN layers with a thickness of about 550 nm measured by SEM. The capacitances and flatband potentials depend on the substrate type. The determined flatband potentials from two different methods (electrochemical impedance spectroscopy and Kelvin probe) considering the experimental errors were in good agreement. The CuSCN deposited on BDD substrate exhibits better blocking function (smaller relative pinhole area) compared to CuSCN deposited on FTO substrate.

ACKNOWLEDGEMENTS

The authors acknowledge the support from the Czech Science Foundation (Contract No. 18-08959S).

REFERENCES

[1] WIJEYASINGHE, N., EISNER, F., TSETSERIS, L. et al. p-Doping of Copper(I) Thiocyanate (CuSCN) Hole-Transport Layers for High-Performance Transistors and Organic Solar Cells. *Advanced Functional Materials*. 2018, vol. 28, pp. 1802055.

[2] NI, Y., JIN, Z., FU, Y. Electrodeposition of p-Type CuSCN Thin Films by a New Aqueous Electrolyte With Triethanolamine Chelation. *Journal of the American Ceramic Society*. 2007, vol. 90, no. 9, pp. 2966-2973.

[3] SUN, L., ICHINOSE, K., SEKIYA, T., et al. Cathodic Electrodeposition of p-CuSCN Nanorod and Its Dye-Sensitized Photocathodic Property. *Phys. Proc*. 2011, vol. 14, pp. 12.

[4] PERERA, V.P.S., SENEVIRATHNA, M.K.I., PITIGALA, P.K.D.D.P., et al. Doping CuSCN Films for Enhancement of Conductivity: Application in Dye-Sensitized Solid-State Solar Cells. *Sol. Energy Mater. Sol. Cells*. 2005, vol. 86, pp. 443.

[5] KAVAN, L., ŽIVCOVÁ, Z.V., HUBÍK, P., et al. Electrochemical Characterization of CuSCN Hole-Extracting Thin Films for Perovskite Photovoltaics. *ACS Applied Energy Materials*. 2019, vol. 2, pp. 4264-4273.

[6] MATEBESE, F., TAZIWA, R., MUTUKWA, D. Progress on the Synthesis and Application of CuSCN Inorganic Hole Transport Material in Perovskite Solar Cells. *Materials*. 2018, vol. 11, pp. 2592.

[7] CHAPPAZ-GILLOT, C., SALAZAR, R., BERSON, S., et al. Room temperature template-free electrodeposition of CuSCN nanowires. *Electrochemistry Communications*. 2012, vol. 24, pp. 1-4.

[8] SUN, L., HUANG, Y., ANOWER HOSSAIN, M., et al. Fabrication of TiO2/CuSCN Bulk Heterojunctions by Profile-Controlled Electrodeposition. *Journal of The Electrochemical Society*. 2012, vol. 159, pp. D323-D327.

[9] RAMÍREZ, D., ÁLVAREZ, K., RIVEROS, G., et al. Electrodeposition of CuSCN seed layers and nanowires: A microelectrogravimetric approach. *Electrochimica Acta*. 2017, vol. 228, pp. 308-318.

[10] SHLENSKAYA, N.N., TUTANTSEV, A.S., BELICH, N.A., et al. Electrodeposition of porous CuSCN layers as hole-conducting material for perovskite solar cells. *Mendeleev Communications*. 2018, vol. 28, pp. 378-380.

[11] YANG, I.S., SOHN, M.R., SUNG, S.D., et al. Formation of pristine CuSCN layer by spray deposition method for efficient perovskite solar cell with extended stability. *Nano Energy*. 2017, vol. 32, pp. 414-421.

[12] CHAVHAN, S., MIGUEL, O., GRANDE, H.J., et al. Organo-metal halide perovskite-based solar cells with CuSCN as the inorganic hole selective contact. *Journal of Materials Chemistry A*. 2014, vol. 2, pp. 12754-12760.

[13] ARORA, N., DAR, M.I., HINDERHOFER, A., et al. Perovskite solar cells with CuSCN hole extraction layers yield stabilized efficiencies greater than 20%. *Science,* 2017. vol. 358, pp. 768-771.

[14] ŽIVCOVÁ, Z.V., PETRÁK, V., FRANK, O., et al. Electrochemical impedance spectroscopy of polycrystalline boron-doped diamond layers with hydrogen and oxygen terminated surface. *Diamond and Related Materials*. 2015, vol. 55, pp. 70-76.

[15] HANKIN, A., ALEXANDER, J.C., KELSALL, G.H. Constraints to the flat band potential of hematite photo-electrodes. *Physical Chemistry Chemical Physics*. 2014, vol. 16, pp. 16176-16186.

[16] BONNET, J., SOONCKINDT, L., LASSABATÈRE, L. The Kelvin probe method for work function topographies: technical problems and solutions. *Vacuum*. 1984, vol. 34, pp. 693-698.

[17] BEERBOM, M.M., LÄGEL, B., CASCIO, A.J., et al. Direct comparison of photoemission spectroscopy and in situ Kelvin probe work function measurements on indium tin oxide films. *Journal of Electron Spectroscopy and Related Phenomena*. 2006, vol. 152, pp. 12-17.

[18] ŽIVCOVÁ, Z.V., FRANK, O., PETRÁK, V., et al. Electrochemistry and in situ Raman spectroelectrochemistry of low and high quality boron-doped diamond layers in aqueous electrolyte solution. *Electrochimica Acta*. 2013, vol. 87, pp. 518-525.

[19] MACPHERSON, J.V. A practical guide to using boron-doped diamond in electrochemical research. *Physical Chemistry Chemical Physics*. 2015, vol. 17, pp. 2935-2949.

[20] KAVAN, L., VLCKOVA ZIVCOVA, Z., PETRAK, V., et al. Boron-doped Diamond Electrodes: Electrochemical, Atomic Force Microscopy and Raman Study towards Corrosion-modifications at Nanoscale. *Electrochimica Acta*. 2015, vol. 179, pp. 626-636.

[21] VLČKOVÁ ŽIVCOVÁ, Z., MORTET, V., TAYLOR, A., et al. Electrochemical characterization of porous boron-doped diamond prepared using SiO_2 fiber template. *Diamond and Related Materials*. 2018, vol. 87, pp. 61-69.

[22] ACHATZ, P., BUSTARRET, E., MARCENAT, C., et al. Metal–insulator transition and superconductivity in highly boron-doped nanocrystalline diamond films. *physica status solidi (a)*. 2009, vol. 206, pp. 1978-1985.

[23] KAVAN, L., TÉTREAULT, N., MOEHL, T., et al. Electrochemical Characterization of TiO_2 Blocking Layers for Dye-Sensitized Solar Cells. *The Journal of Physical Chemistry C*. 2014, vol. 118, pp.16408-16418.